Effect of Diffusion Interactions between Droplets on Gas Absorption of Highly Soluble Gases in Sprays and Droplet Clusters

T. Elperin, A. Fominykh and B. Krasovitov *
Department of Mechanical Engineering
The Pearlstone Center for Aeronautical Engineering Studies
Ben-Gurion University of the Negev, P. O. B. 653, 84105, Israel
elperin@bgu.ac.il, fominykh@bgu.ac.il and borisk@bgu.ac.il

Abstract

We investigate mass transfer during absorption of highly soluble gases such as HNO_3, H_2O_2 by droplets in clusters and sprays in the presence of inert admixtures. Diffusion interactions between droplets, caused by the overlap of depleted of soluble gas regions around the neighboring droplets, are taken into account in the approximation of a cellular model of a gas-droplet suspension whereby a suspension is viewed as a periodic structure consisting of the identical spherical cells with periodic boundary conditions at the cell boundary. Using this model we determined temporal and spatial dependencies of the concentration of the soluble gas in a gaseous phase and in a droplet. The suggested model was also extended for describing gas absorption by atmospheric cloud droplets. We found that scavenging coefficient for gas absorption by cloud droplets remains constant and sharply decreases only at the final stage of absorption. In the calculations we employed a Monte Carlo method and assumed gamma size distribution of cloud droplets. It was shown that despite of the comparable values of Henry's law constants for the hydrogen peroxide (H_2O_2) and the nitric acid (HNO_3), the nitric acid is scavenged more effectively by cloud droplets than the hydrogen peroxide due to a major affect of the dissociation reaction on HNO_3 scavenging.

Introduction

Absorption air pollution control processes include wet removal of moderately and highly soluble gases by dispersed liquid phase in various types of packed and spray towers and in-cloud scavenging of highly soluble gases. Soluble gas absorption by small droplets without internal circulation was investigated experimentally in [1]. Gas absorption in the presence of inert admixtures, in the case when both phases affect mass transfer, was analyzed theoretically in [2] – [3].

Spray absorption and spray absorber design and analysis attracted considerable attention in recent years because of higher contact surfaces per unit volume and higher rates of mass transfer in spray absorbers in comparison with conventional falling film absorbers. In the past, many experimental and theoretical studies have been carried out to examine the mass transfer characteristics of spray towers and scrubbers for various gas–liquid systems (see. e.g., [4] – [7]). In [6] theoretical model for flue gas desulfurization by spray-dry absorption with lime slurry was developed. The model combines a steady state one-dimensional spray-dryer model with a single-drop model for SO_2 absorption with the instantaneous irreversible reaction in a rigid droplet containing uniformly dispersed fine lime particles. Theoretical model for water scrubbing under laminar flow was suggested in [5]. In this study the removal efficiency of SO_2 in a spray tower is considered as the result of the collective absorbing capacities of all the droplets in the tower. Kinetic and mass-transfer behaviour of spray-tower-loop absorbers and reactors was investigated experimentally in [7] where it was showed that the internally well-mixed drops model is more reliable. Moderately fast reactions do not affect mass transfer, while extremely fast reactions require the introduction of the enhancement factor.

Scavenging of soluble gases by single evaporating droplets was analyzed in [8] – [9]. In-cloud scavenging of highly-soluble gases was investigated in [10] – [12]. In [10] it is assumed that soluble gas scavenging by cloud droplets is governed by physical absorption. Assuming that droplet size distribution in a cloud is determined by empirical distribution the authors determined the value of the scavenging coefficient, $\Lambda = 0.2\ \mathrm{s}^{-1}$, and the characteristic time for dissolution of gaseous HNO_3, $\tau = 5\ \mathrm{s}$, in a cloud. The influence of the fine microphysical features such as droplet size distribution and liquid water content on in-cloud scavenging was analyzed also in [12]. Different aspects of scavenging of soluble gases by cloud droplets were discussed also in [13]–[14]. It must be emphasized that in all above mentioned studies mass transfer during gas absorption by droplets was investi-

* Corresponding author: borisk@bgu.ac.il

gated neglecting interaction between the neighboring droplets. This approach allows determining evolution of the concentration of the dissolved gas in a droplet.

Heat and mass transfer in sprays is complex problem that involves the effects of turbulence, droplet motion, coagulation, breakup etc. Nevertheless, the studies of the diffusion interaction between droplets in stagnant clusters provide a fundamental knowledge of the processes that occur in atomization and spray systems (see e.g., [15]). Moreover, the model of gas absorption by stagnant droplet clusters adequately describes gas absorption by mist formed in gas streams inside gas absorbers and scavenging of atmospheric soluble gases. In the present study we investigate gas absorption of highly soluble gas by stagnant droplet clusters as well as atmospheric clouds. Interaction between droplets is accounted for by employing the cellular model of the dispersed media (see e.g. [16]). In this model the individual droplets in the cluster are considered to be located at the center of a unit cell whereas the whole cluster is described by a cellular structure. Consequently, in this model it is sufficient to analyze mass transfer in a unit cell in order to describe mass transfer in a droplet cluster.

Mathematical model

In contrast to absorption of slightly soluble gases by sprays and clusters, for highly soluble gases, e.g., HNO_3, H_2O_2 the total amount of a soluble gas that can be dissolved in the droplets can be of the same order of magnitude or larger than the total amount of the soluble gas in a cloud. Therefore, gas absorption by droplets results in the overlap of the depleted of soluble gas regions around the droplets, and their diffusion interaction must be taken into account. Interactive absorption by droplets during the uptake of soluble gas can be adequately described in the approximation of a cellular model of the dispersed media (see Fig. 1). Assuming that the volumetric liquid water content in the droplet cluster or cloud is φ_L, let us consider a model whereby each droplet is embedded into the gaseous spherical shell with the radius R. This radius is determined by the relation:

$$\varphi_L = a^3 / R^3, \tag{1}$$

where a is a radius of a spherical droplet located at the center of the cell. Assume that the mass fluxes at the cell boundary vanish. The latter condition will apparently be fulfilled at a finite number of the boundary points because in the middle of the straight line connecting the centers of the neighboring cells the mass fluxes to the droplets will be equal in magnitude but opposite in direction [17].

Consider a droplet immersed into a stagnant gaseous mixture. The gaseous mixture contains the inert gas and soluble species that is absorbed into the liquid droplet. In further analysis we assume spherical symmetry. Extending the conditions of vanishing mass flux to the entire cell boundary we arrive at the following set of equations which describe the process:

In the liquid phase, $0 < r < a$,
$$\frac{\partial C_{A,L}}{\partial t} = D_{A,L}\nabla^2 C_{A,L}, \tag{2}$$

In the gaseous phase, $a < r < R$,
$$\frac{\partial C_{A,G}}{\partial t} = D_{A,G}\nabla^2 C_{A,G}. \tag{3}$$

The initial conditions for the system of equations (2) and (3) read:

$$t = 0: \; C_{A,L} = 0, \; C_{A,G} = C_0. \tag{4}$$

The conditions of the continuity of mass flux at the gas-liquid interface yields:

$$D_{A,L}\left.\frac{\partial C_{A,L}}{\partial r}\right|_{r=a} = D_{A,G}\left.\frac{\partial C_{A,G}}{\partial r}\right|_{r=a}. \tag{5}$$

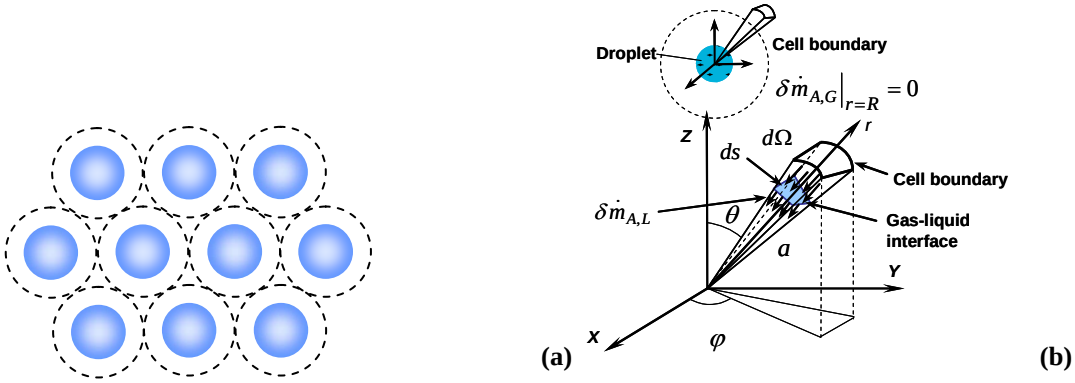

Figure 1 (a) Schematic view of cellular structure; (b) system of coordinate and fluxes.

It must be noted that the boundary condition (5) is valid in the case when the flux of the molecules which are not absorbed at the droplet surface and leave the surface back into the gas can be neglected. The boundary condition for the concentration of the absorbate at the surface of the droplet can be obtained from the analysis of the dissociation reactions. The following equilibrium reactions occur when gaseous HNO_3 is dissolved in a water droplet (see, e.g., [18], pp. 299 – 302):

$$HNO_3(g) + H_2O \overset{H_{HNO_3}}{\rightleftarrows} HNO_3 \cdot H_2O, \qquad H_{HNO_3} = \frac{[HNO_3 \cdot H_2O]}{p_{HNO_3}}, \tag{6}$$

$$HNO_3 \cdot H_2O \overset{K_1}{\rightleftarrows} H^+ + NO_3^-, \qquad K_1 = \frac{[H^+][NO_3^-]}{[HNO_3 \cdot H_2O]}, \tag{7}$$

where $HNO_3 \cdot H_2O$ is physically-dissolved HNO_3, NO_3^- is the nitrate, H_{HNO_3} is the Henry's constant and K_1 is the dissociation constant. For the total concentration of the dissolved nitric acid we obtain the following expression:

$$[N(V)] = [HNO_3 \cdot H_2O] + [NO_3^-]. \tag{8}$$

Using the Henri law we obtain:

$$[HNO_3 \cdot H_2O] = H_{HNO_3} \cdot p_{HNO_3}. \tag{9}$$

Equation (9) and the dissociation equilibrium equations (7) – (8) yield:

$$[N(V)] = H^*_{HNO_3} \cdot p_{HNO_3} = H_{HNO_3} \cdot \left(1 + \frac{K_1}{[H^+]}\right) \cdot p_{HNO_3}, \tag{10}$$

where $H^*_{HNO_3} = H_{HNO_3}\left(1 + K_1/[H^+]\right)$ is the effective Henry's law coefficient for the nitric acid. Since $K_1/[H^+] >> 1$, Eq. (10) implies that

$$[N(V)] = p_{HNO_3} \cdot H_{HNO_3} \cdot K_1/[H^+]. \tag{11}$$

Taking into account that

$$[NO_3^-] = \frac{K_1 \cdot H_{HNO_3} \cdot p_{HNO_3}}{[H^+]}, \quad [H^+] = \sqrt{K_1 \cdot H_{HNO_3} \cdot p_{HNO_3}} \tag{12}$$

we arrive at the following relation at the surface of a droplet:

$$C_{A,L} = \sqrt{K_{A,0} C_{A,G} \cdot R_g T}, \tag{13}$$

where $K_{A,0} = H_{HNO_3} \cdot K_1 = 3.3 \cdot 10^6 \exp\left(-8700(1/298 - 1/T)\right)$ $\left(\text{mol}^2\ \text{l}^{-2}\ \text{atm}^{-1}\right)$.

The boundary conditions in the center of the droplet and at the cell boundary read:

$$\left.\frac{\partial C_{A,L}}{\partial r}\right|_{r \to 0} = 0, \quad \left.\frac{\partial C_{A,G}}{\partial r}\right|_{r=R} = 0. \tag{14}$$

Conditions (14) reflect the requirement that the droplet center should be neither a sink nor a source for the absorbate and the fact that due to the periodicity condition mass flux at the cell boundary vanishes. Therefore absorption of soluble gas in a cluster is described by the system of equations (2) – (3) with the initial and boundary conditions (4), (5), (13) – (14).

Inspection of Eqs. (2) – (3) reveals that the problem is formulated in two computational domains, $0 < r < a$ for the liquid phase and $a < r < R$ for the gaseous phase. Moreover, the characteristic times of the heat and mass transfer in the gaseous phase and heat transfer in the liquid phase are considerably smaller than the characteristic time of the diffusion of soluble component in liquid. In order to overcome these problems, we introduced the following dimensionless time, $\tau = D_{A,L}\, t / a^2$. Then the governing equations can be rewritten for time variable τ using the following coordinate transformations: $x = 1 - r/a$ for the domain $0 \le r \le a$ and $w = \sigma^{-1}(r/a - 1)$ for the domain $a \le r \le R$. The parameter σ is chosen such that the coordinate *w* equals 1 at the boundary of the cell. In the transformed computational domains the coordinates, x and w, vary in the same range, $x \in [0, 1]$, $w \in [0, 1]$, and can be treated identically in the numerical calculations. The gas-liquid interface is located at $x = w = 0$. The obtained system of parabolic partial differential equations was solved using the method of lines [19]. The mesh points were spaced adaptively using the following formula:

$$x_i = \left(\frac{i-1}{N}\right)^n, \qquad i = 1,\ldots,N+1. \tag{15}$$

Equation (15) implies that mesh points cluster near the left boundary where the gradients are steep. In Eq. (15) N is the chosen number of mesh points, n is an integer coefficient (in our calculations n is chosen equal to 3). The resulting system of ordinary differential equations was solved using a backward differentiation method. Generally, in the numerical solution, 151 mesh points and an error tolerance ~ 10^{-5} in time integration were employed. Variable time steps were used to improve the computing accuracy and efficiency.

Taking into account dissociation reactions in a liquid droplet and Eq. (13) we can also obtain the following expressions for the "equilibrium values" of the concentration of the active gas in the gaseous phase and for the total concentration of the nitric acids in the liquid phase:

$$C_{Geq} = \frac{1}{2}\left[\Phi + 2C_{G,0} - \sqrt{\Phi}\sqrt{\Phi + 4C_{G,0}}\right], \tag{16}$$

$$C_{L,[\mathrm{N(V)}]\,eq} = \frac{1}{\sqrt{2}}\left(K_{A,0}R_gT\left[\Phi + 2C_{G,0} - \sqrt{\Phi}\sqrt{\Phi + 4C_{G,0}}\right]\right)^{1/2}, \tag{17}$$

where $\Phi = K_{A,0}R_gT\varphi_L^2/(1-\varphi_L^2)$. Taking into consideration that $[\mathrm{N(V)}] \approx [\mathrm{H}^+]$ we arrive at the following formula for pH in a saturated droplet:

$$\mathrm{pH} = -\log\left([\mathrm{H}^+]_0 + C_{L,[\mathrm{N(V)}]eq}\right), \tag{18}$$

where $[\mathrm{H}^+]_0$ is the initial concentration of the ions $[\mathrm{H}^+]$ in a cloud droplet.

The equilibrium reactions occurring when the hydrogen peroxide (H_2O_2) is dissolved in water are similar to the reactions of dissolution of the nitric acid (HNO_3). Hydrogen peroxide dissociates to produce ions HO_2^-:

$$\mathrm{H_2O_2(g) + H_2O \overset{H_{H_2O_2}}{\rightleftarrows} H_2O_2 \cdot H_2O}, \tag{19}$$

$$\mathrm{H_2O_2 \cdot H_2O \overset{K_{1,H_2O_2}}{\rightleftarrows} H^+ + HO_2^-}. \tag{20}$$

However in contrast to the nitric acid solution, the hydrogen peroxide solution in water is a weak electrolyte with the dissociation constant $K_{1,\mathrm{H_2O_2}} = 2.2\cdot10^{-12}$ M at the temperature 298 K. It was shown (see e.g., [18], pp. 302-303) that $\dfrac{[\mathrm{HO_2^-}]}{[\mathrm{H_2O_2 \cdot H_2O}]} = \dfrac{K_{1,\mathrm{H_2O_2}}}{[\mathrm{H^+}]} < 10^{-4}$ for pH values less than 7.5. Therefore for most applications the dissociation of H_2O_2 in water can be neglected, and the dissolution of the hydrogen peroxide in water obeys the Henry's law. Consequently, when H_2O_2 absorption by a water droplet is completed, the concentration of the soluble gas in the gaseous phase decreases from the initial value C_{G0} down to the "equilibrium value":

$$C_{Geq} = \frac{C_{A,G0}(1-\varphi_L)}{1+\varphi_L(H_{\mathrm{H_2O_2}}R_gT-1)}, \tag{21}$$

where R_g is the universal gas constant. Accordingly, the concentration of the dissolved gas in the droplet increases from zero up to the "equilibrium value":

$$C_{Leq} = \frac{H_{\mathrm{H_2O_2}}R_gT\cdot C_{A,G0}(1-\varphi_L)}{1+\varphi_L(H_{\mathrm{H_2O_2}}R_gT-1)}. \tag{22}$$

Results and Discussion

The cellular model of gas absorption by clusters was applied to study the temporal and spatial dependencies of the soluble gas concentration inside the droplets and in a gaseous phase. The results of the numerical solution of the system of equations (2) – (3) with the initial and boundary conditions (4) – (5), (13) and for the uniform initial distribution of the soluble gas in the gaseous phase are shown in Figs. 2 – 7.

Calculations are performed for absorption of highly soluble gases by water droplets taking into account the dissociation reactions in the liquid phase. The dependencies of the total concentration $[\mathrm{N(V)}]$ of the nitric acids and pH in a liquid phase vs. time and radial coordinate are shown in Fig. 2. Calculations were performed for the ambient temperature 298 K and for the initial concentrations of the nitric acid in a gaseous phase 63.4 μg/m^3 and droplets' radii 10 μm. Inspection of Fig. 2 shows that if the initial concentration of the nitric acid in the gaseous

phase is equal to 63.4 μg/m^3 , the acidity of the aqueous solution pH in the droplet varies in the range from 5.5 to 2.7.

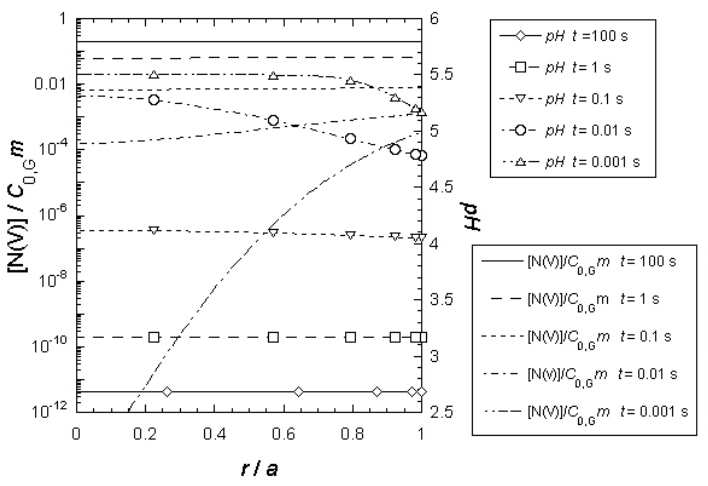

Figure 2 Dependence of the total concentration, $[\mathrm{N(V)}]$, of the nitric acids and pH in a liquid phase vs. time and radial coordinate ($C_{G,0} = 63.4$ μg/m^3 , $m = H_{\mathrm{HNO_3}} R_g T$).

The dependencies of the dimensionless concentration of the soluble gas (HNO_3) in the gaseous phase vs. time and radial coordinate are shown in Fig. 3. Calculations were performed for cloud of droplets with radii 10 μm immersed into the gaseous phase with the ambient temperature 298 K and the initial concentration of gaseous nitric acid 63.4 μg/m^3. Inspection of Fig. 3 shows that the depleted by soluble gas region around the droplet extends from the surface of the droplet to the boundary of a cell. Fig. 3 imply that for large time the concentration of HNO_3 in the gaseous phase can be determined by Eq. (16).

In Fig. 4 we showed the dependencies of pH in the saturated droplets vs. the initial concentration of HNO_3 in the gaseous phase. Calculations were performed using Eqs. (17)–(18) for the ambient temperature 298 K and different values of liquid water content in a cloud. As can be seen from this plot the pH in saturated cloud droplets decreases when the liquid water content decreases.

We also applied the suggested model for the investigation of gas absorption by atmospheric cloud droplets. The dependencies of the average normalized concentration of HNO_3 in the gaseous phase, the rate of concentration change $d\bar{c}/dt$ and the scavenging coefficient vs. time are shown in Fig. 5. The curves are plotted for the volume fraction of droplets in a cloud $\varphi_L = 10^{-6}$. This magnitude of the volume fraction of droplets, $\varphi_L = 10^{-6}$, implies that 1 m^3 of air contains 1.0 cm^3 of water. The average concentration of HNO_3 in the gaseous phase was calculated as follows:

$$\overline{C}_G = \frac{1}{V_c - V_d} \int C_{A,G}(r)\, r^2 \sin\vartheta \, dr \, d\vartheta \, d\varphi \,, \tag{23}$$

where V_c and V_d are the cell and droplet volumes, correspondingly, r , ϑ and φ are the spherical coordinates. The calculations showed in Fig. 5 were performed for cloud droplets with the radii of 5 and 10 μm, correspondingly, and for the fixed volume fraction of droplets 10^{-6}.

We also calculated the scavenging coefficient for the soluble trace gas absorption from the atmosphere:

$$\Lambda = -\frac{1}{\bar{c}} \frac{\partial \bar{c}}{\partial t} \,. \tag{24}$$

As can be seen from these plots the scavenging coefficient remains constant, and sharply decreases at the final stage of gas absorption. This assertion implies exponential time decay of the average concentration of the soluble trace gas in the gaseous phase. The latter conclusion can be used for parameterization of gas scavenging by cloud droplets in the atmospheric transport modeling similarly to the aerosol wet deposition (see e.g. [20]).

As can be seen from Fig. 5 for the fixed value of volume fraction of droplets equal to 10^{-6} the scavenging coefficient in the cloud increases when the droplet radius decreases. This tendency is caused by the increase of the gas-liquid contact surface per unit volume as the droplet radius decreases. We also calculated the rate of concentration change as a function of time (see Fig. 5).

The dependencies of the scavenging coefficient as a function of time for different values of the initial concentration of the soluble trace gas in the gaseous phase are shown in Fig. 6. As can be seen from these plots in the case of the fixed value of the volume fraction of droplets in the cloud and droplet radii, the magnitude of the initial concentration of trace gas in the gaseous phase affects the scavenging coefficient only at the final stage of gas absorption.

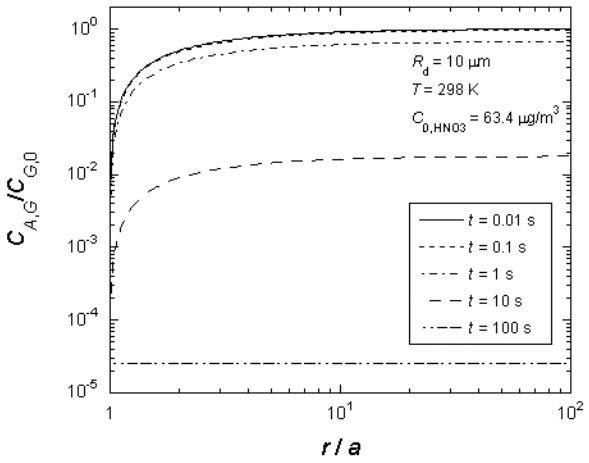

Figure 3 Dependence of the concentration of the soluble gas (HNO_3) in the gaseous phase vs. time and radial coordinate ($C_{G,0} = 63.4\ \mu g/m^3$).

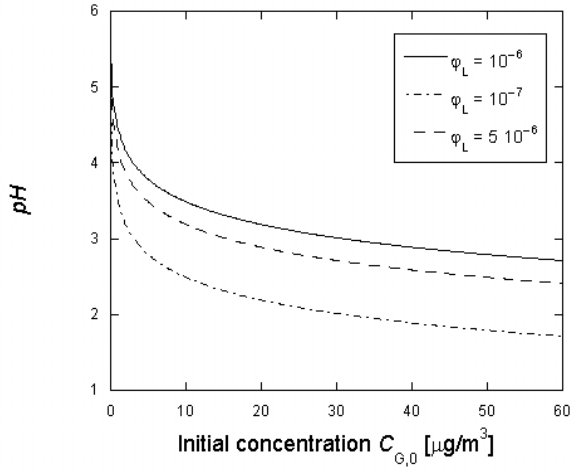

Figure 4 Dependence of pH in the saturated droplet vs. initial concentration of HNO_3 in the gaseous phase for different values of liquid water content in a cloud.

Notably, when dissociation in water can be neglected (e.g., in the case of H_2O_2 absorption in a liquid phase) scavenging coefficient is independent of the magnitude of the initial concentration of the trace gas in the gaseous phase.

The dependence of the scavenging coefficient for the nitric acid (HNO_3) absorbed by cloud droplets vs. time taking into account droplet size distribution in the cloud is shown in Fig. 7. In the calculations we assumed the gamma size distribution of cloud droplets with the following probability density function:

$$f(a) = \frac{1}{\Gamma(\alpha+1)\,\beta^{\alpha+1}}\, a^{\alpha} \exp\left(-\frac{a}{\beta}\right), \tag{25}$$

where a is the radius of the droplet, α is the shape parameter and β is the scale parameter. The scale parameter β can be determined as follows: $\beta = \bar{a}/(\alpha+1)$, where $\bar{a}$ is the average radius of the droplets and the shape parameter $\alpha = 6$ (see e.g., [21]). Droplet size distribution was taken into account using the Monte Carlo method whereby the scavenging coefficient was calculated by solving the initial boundary-value problem (2) – (3) for a droplet radius that was randomly sampled from the probability density function (25). The scavenging coefficient is determined by averaging the obtained 1000 scavenging coefficients at each time step. Calculations were performed for the average radii 4.7 μm. Calculations were performed for different average radii but for the same volume fraction of droplets in a cluster, $\varphi_L = 10^{-6}$.

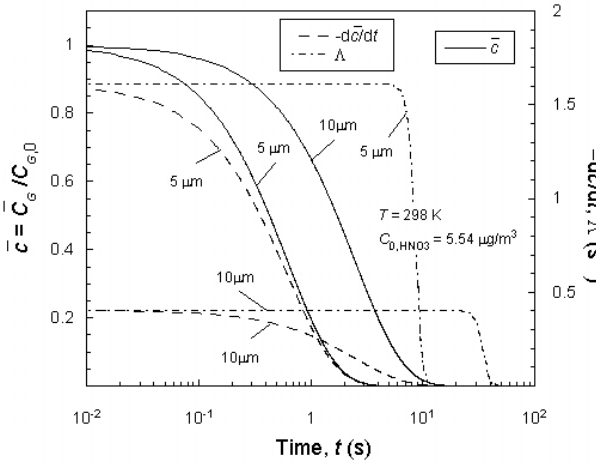

Figure 5 Dependence of the average normalized concentration of HNO_3 in the gaseous phase, the rate of concentration change $-d\bar{c}/dt$ and scavenging coefficient vs. time ($\varphi_L = 10^{-6}$, $C_{G,0} = 5.54\ \mu g/m^3$).

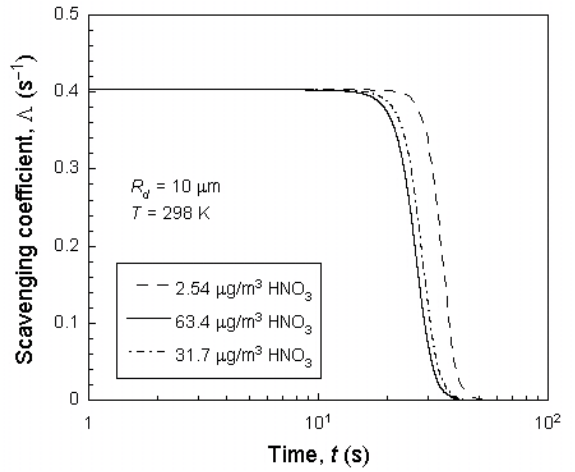

Figure 6 Dependence of the scavenging coefficient of HNO_3 vs. time for different values of the initial concentration of soluble trace gas in the gaseous phase.

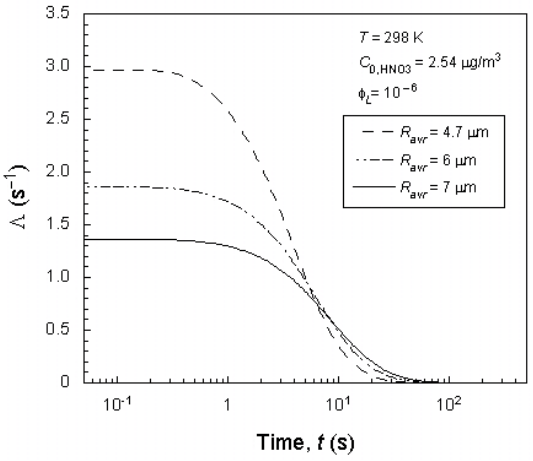

Figure 7 Dependence of the scavenging coefficient for the nitric acid HNO_3 on time taking into account gamma droplet size distribution in a cloud.

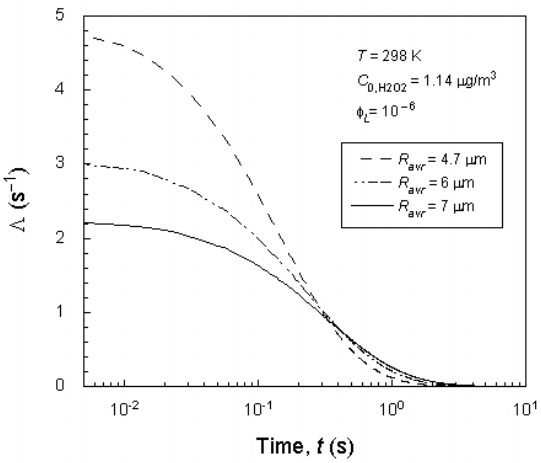

Figure 8 Dependence of scavenging coefficient for the hydrogen peroxide H_2O_2 on time taking into account gamma droplet size distribution in a cloud.

As can be seen from Fig. 7 the scavenging coefficient in the cloud increases when the droplet radius decreases. This tendency is caused by the increase of the gas-liquid contact surface area per unit volume as the droplet radius decreases. Similar calculations were performed for the hydrogen peroxide H_2O_2 scavenged by cloud droplets (see Fig. 8). Calculations were conducted for average radii 4.7 μm, 6 μm and 7 μm and for the constant volume fraction of droplets in a cloud, $\varphi_L = 10^{-6}$.

The "equilibrium fraction" of the total hydrogen peroxide (H_2O_2) and nitric acid (HNO_3) in the gaseous phase as a function of liquid water content is shown in Fig. 9. These calculations were performed for the ambient temperature 298 K. Here the term "equilibrium fraction" denotes the ratio of the soluble trace gas concentration in the gaseous phase in a state when gas absorption is completed to the initial concentration of the soluble trace gas in the cloud interstitial air.

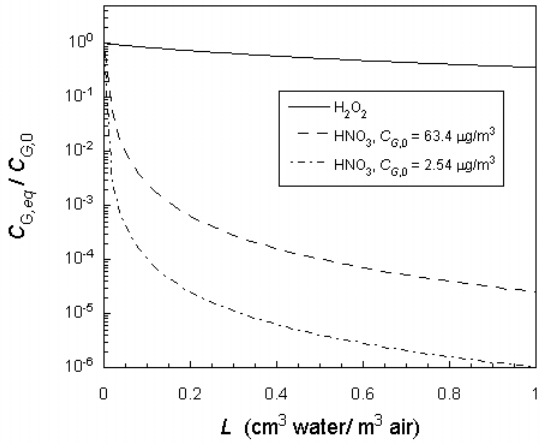

Figure 9. Equilibrium fraction of the total hydrogen peroxide (H_2O_2) and nitric acid (HNO_3) in the gaseous phase as a function of liquid water content at 298 K.

As can be seen from this plot for a cloud liquid water content of 1.0 g/m^3 (i.e., $\varphi_L = 10^{-6}$), approximately 40% of the hydrogen peroxide is scavenged by the cloud droplets. Equations (21) – (22) imply that the "equilibrium fraction" of the total H_2O_2 does not depend on the initial concentration of H_2O_2 in the ambient air. The latter conclusion is the result of the minor role played by dissociation in the process of hydrogen peroxide absorption by cloud droplets. Despite of the comparable values of the Henry's law constants for the hydrogen peroxide and the nitric acid the nitric acid is scavenged more effectively by cloud droplets than the hydrogen peroxide (see Fig. 9). The latter assertion results from the major role played by dissociation during absorption of nitric acid by cloud droplets.

As can be seen from Fig. 9 the "equilibrium fraction" of the nitric acid depends on the initial concentration of HNO_3 in the gaseous phase. However, inspection of this figure shows that for a cloud liquid water content of 1.0 g/m^3 only a negligibly small amount of HNO_3 remains in the cloud interstitial air even in the case of fairly high atmospheric concentrations of HNO_3 in the ambient air e.g., 63.4 μg/m^3.

Summary and Conclusions

We accounted for the diffusion interactions between droplets in a cloud caused by the overlap of depleted of soluble gas regions around droplets using the cellular model of a gas-droplet suspension whereby a suspension is viewed as a periodic structure consisting of the identical spherical cells with the periodic boundary conditions at the cell boundary. The suggested model assumes that gas absorption by droplets is accompanied by the subsequent aqueous-phase equilibrium dissociation reaction. The initial boundary value problem was solved using the

method of lines and Monte Carlo simulations. In the calculations of gas absorption by cloud droplets we assumed gamma size distribution of cloud droplets. We obtained also the analytical expressions for the "equilibrium values" of concentration of the active gas in a gaseous phase and for the total concentration in the liquid phase for the case of H_2O_2 and HNO_3 absorption by droplets. The results obtained in this study allow us to draw the following conclusions:

- Gas absorption of highly soluble gases by clusters causes a significant decrease of the soluble gas concentration in the interstitial air. Calculations conducted for the hydrogen peroxide (H_2O_2) and the nitric acid (HNO_3) showed that in spite of the comparable values of the Henry's law constants for H_2O_2 and HNO_3, the nitric acid is absorbed more effectively than the hydrogen peroxide. It is demonstrated that for a cloud with liquid water content of 1.0 g/m^3 approximately 40% of H_2O_2 is scavenged by cloud droplets while only a negligibly small amount of HNO_3 remains in the cloud interstitial air even in the case of fairly high atmospheric concentrations of HNO_3 in the ambient air such as 63.4 μg/m^3. Consequently, the chemical dissociation reaction affects not only the concentration of the dissolved gas in the droplet but also the concentration of the soluble gas in the interstitial gas.
- Using the suggested cellular model we determined the dependencies of the scavenging coefficient as a function of time for different values of the initial concentration of the nitric acid in the atmosphere. It was found that scavenging coefficient remains constant and sharply decreases only at the final stage of gas absorption. This assertion implies the exponential time decay of the average concentration of the soluble gas in the gaseous phase and can be used for the parameterization of gas scavenging by cloud droplets in the atmospheric transport modeling.
- Using the suggested model we calculated temporal evolution of pH in cloud droplets. It was shown that pH strongly depends on the liquid content in the cloud and on the initial concentration of the soluble trace gas in the gaseous phase.

The results of the present study can be useful in an analysis of different meteorology-chemistry models and in particular in various parameterizations of the in-cloud scavenging of the atmospheric soluble gases. Analysis of the diffusion interaction between droplets in stagnant droplet clusters provides a fundamental knowledge of the processes that occur in atomization and spray systems. Moreover the suggested model of gas absorption by stagnant droplet clusters adequately describes gas absorption by mist formed in gas streams inside gas absorbers and scavenging of atmospheric soluble gases.

References

[1] Taniguchi, I., and K. Asano, *Journal of Chemical Engineering of Japan* 25: 614–616 (1992).
[2] Clift, R., Grace, J.R., and M.E. Weber, *Bubbles, Drops and Particles*, Academic Press, NY, 1978.
[3] Plocker, U. J., and H. Schmidt-Traub, *Chemie Ingenieur Techn*ik 44: 313–319 (1972).
[4] Javed, K.H., Mahmud, T. and Purba, E., *Chemical Engineering Journal* 162: 448–456 (2010).
[5] Bandyopadhyay, A., Biswas, M. N., *Science of the Total Environment* 383: 25–40 (2007).
[6] Scala F., D'Ascenzo M. and Lancia, A., *Separation and Purification Technology* 34: 143–153 (2004).
[7] Dimiccoli, A., Di Serio, M. and Santacesaria, E., *Ind. Eng. Chem. Res.* 39-11: 4082–4093 (2000).
[8] Elperin, T., Fominykh, A. and Krasovitov, B., *Journal of the Atmospheric Sciences* 64: 983–995 (2007).
[9] Elperin, T., Fominykh, A., and Krasovitov, B., Atmospheric Environment 42, 3076–3086 (2008).
[10] Levine S. Z. and Schwartz, S. E., *Atmospheric Environment* 16: 1725-1734 (1982).
[11] Wurzler, S., *Atmospheric Research* 48: 219–233 (1998).
[12] Chaumerliac N., Leriche, M., Audiffren, N., Atmospheric Research 53: 29–43 (2000).
[13] Zhang, L.M., Michelangeli, D.V; Djouad, R.; Taylor, P.A., *Atmospheric Research* 80: 187-217 (2006).
[14] Long, Y., Chaumerliac, N., Deguillaume, L., Leriche, M., Champeau, F., *Atmos. Res.* 97-4: 540-554 (2010).
[15] W.A. Sirignano, *Fluid Dynamics and Transport of Droplets and Sprays*, 2nd ed., Cambridge University Press, 2010.
[16] Happel, J., *AIChE Journal* 4: 197-201 (1958).
[17] Elperin, T., Fominykh, A., *Heat and Mass Transfer* 31-5: 307-313 (1996).
[18] Seinfeld, J.H., and Pandis, S. N., *Atmospheric Chemistry and Physics. From Air Pollution to Climate Change*. Second ed. John Wiley & Sons, NY, 2006.
[19] Sincovec R. F. and Madsen, N. K., *ACM Transactions on Mathematical Software*, 1: 232–260 (1975).
[20] Baklanov, A. and Sørensen J.H., *Physics and Chemistry of the Earth, Part B*, 26-10: 787–799 (2001).
[21] Wyser K., *Atmospheric Research*, 49: 213–234 (1998).